Journal of Materials Chemistry C

ROYAL SOCIETY OF CHEMISTRY

PAPER

View Article Online
View Journal | View Issue

Cite this: J. Mater. Chem. C, 2025, 13, 11970

Croconaine dyes with intermediate diradical character exhibiting intense one- and two-photon absorption in the short-wavelength infrared region†

Taishi Oka,[a] Takeshi Maeda,*[a] Daisuke Sakamaki,[b] Hideki Fujiwara,*[b] Naoya Suzuki,[a] Shintaro Kodama,[a] Shigeyuki Yagi,[a] Luca Mauri[cd] and Kenji Kamada*[c]

Chalcogenopyrylium-based croconaine dyes with intermediate diradical character exhibit intense one-photon absorption (OPA) and two-photon absorption (TPA) in the short-wavelength infrared (SWIR) region. These properties arise from the synergistic effects of enhanced diradical character via substitution with heavier chalcogen atoms (O, S, Se) and π-conjugation extension through sphenyl group incorporation. Chalcogenopyrylium-based croconaine dyes with intermediate diradical character exhibit intense one-photon absorption (OPA) and two-photon absorption (TPA) in the short-wavelength infrared (SWIR) region. These properties arise from the synergistic effects of enhanced diradical character through substitution with heavier chalcogen atoms (O, S, Se) and π-conjugation extension *via* phenyl substitution. X-Ray crystal structure analysis, temperature-dependent ^{1}H-NMR, and ESR spectra revealed the intermediate diradical character of the croconaine dyes, with the contribution of the diradical form increasing in the order O < S < Se as the atomic number of the chalcogen element increases. Correspondingly, the OPA band shifts to lower energy regions. Notably, dyes incorporating sulfur and selenium exhibit strong OPA in the SWIR region, with absorption maxima at 1046 nm and 1096 nm, respectively. Furthermore, TPA spectra measured using the Z-scan technique reveal that dyes containing O, S, and Se exhibit large TPA cross sections of 1008 GM at 1255 nm, 1011 GM at 1395 nm, and 1177 GM at 1445 nm, respectively. The absorption bands shift to lower energy regions, similar to the OPA bands, with the cross section increasing with the atomic number of the chalcogen element. These findings demonstrate that chalcogen atoms not only play a crucial role in modulating the intermediate diradical character of croconaine dyes but also significantly influence their OPA and TPA properties.

Received 5th March 2025,
Accepted 6th May 2025

DOI: 10.1039/d5tc00973a

rsc.li/materials-c

Introduction

Short-wavelength infrared (SWIR) radiation, with wavelengths longer than 1000 nm, exhibits high penetration through a wide range of materials, making it ideal for non-destructive testing in industrial and agricultural applications.[1,2] Its limited scattering and absorption in biological tissues further enhance its potential for deep-tissue imaging and photodynamic therapy.[3–5] These advantageous properties of SWIR motivate the development of materials that efficiently absorb this radiation. While inorganic semiconductors such as InGaAs are effective at absorbing SWIR radiation,[6–8] they contain rare and toxic elements, emphasizing the need for more sustainable and non-toxic alternatives.

Organic materials offer a promising alternative for SWIR absorption, as their structural diversity enables precise tuning of the orbital energy levels involved in electronic transitions.[9–11] SWIR-absorbing organic molecules typically feature an extended π-electron system that links strong electron donors and acceptors.[12–14] This arrangement promotes resonance, where electron push–pull effects between donors and acceptors reduce bond alternation and suppress Peierls distortion, also known as

[a] Department of Applied Chemistry, Graduate School of Engineering, Osaka Metropolitan University, Naka-ku, Sakai, Osaka 599-8531, Japan. E-mail: tmaeda@omu.ac.jp
[b] Department of Chemistry, Graduate School of Science, Osaka Metropolitan University, Sumiyoshi-ku, Osaka 558-8585, Japan. E-mail: hfuji@omu.ac.jp
[c] Nanomaterials Research Institute (NMRI), National Institute of Advanced Industrial Science and Technology (AIST) Ikeda, Osaka 563-8577, Japan. E-mail: k.kamada@aist.go.jp
[d] Chemistry Department, Università degli Studi di Milano, UdR dell'INSTM, Via Golgi 19, Milano 20133, Italy

† Electronic supplementary information (ESI) available: Synthetic procedures, experimental details. CCDC 2407572 (**CR2c**). For ESI and crystallographic data in CIF or other electronic format see DOI: https://doi.org/10.1039/d5tc00973a

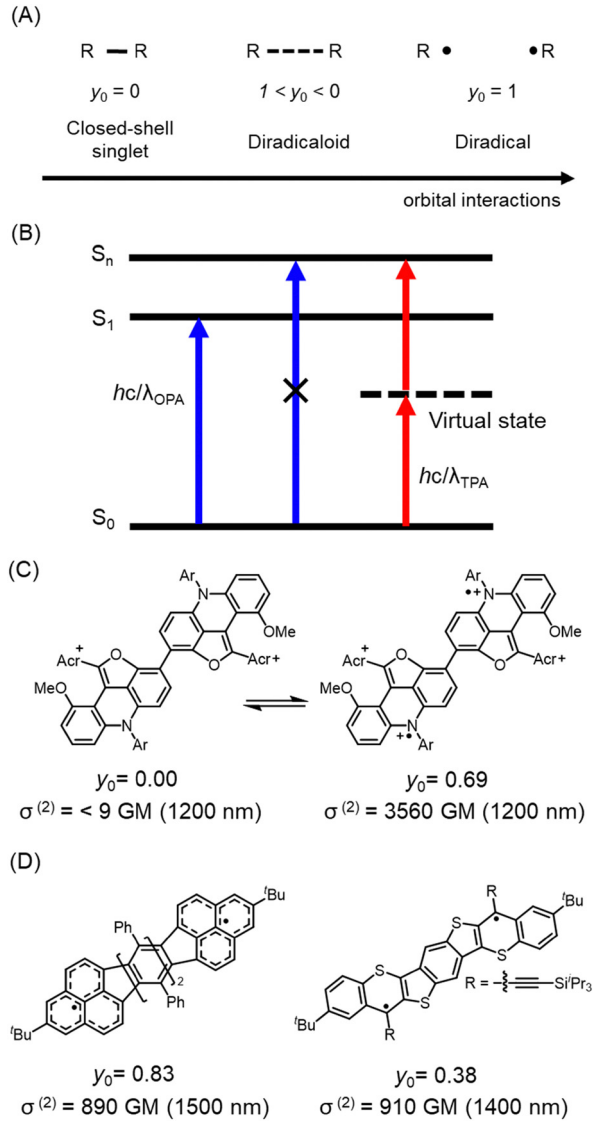

Fig. 1 (A) Correlation between orbital interactions and electronic structure: The closed-shell electronic structure resulting from orbital interactions (left, diradical character y_0 = 0), the open-shell electronic state without orbital interactions (right, y_0 = 1), and the intermediate state between the closed-shell and open-shell configurations (center, 0 < y_0 < 1). (B) Three-state model of the TPA process, consisting of the ground state, virtual state, and excited state, where the one-photon transition is forbidden and the two-photon transition is allowed in symmetric molecular systems. (C) TPA cross-section ($\sigma^{(2)}$), with the maximum absorption wavelength for TPA in parentheses, for the bis(acridine) dimer (left) and its oxidized state with intermediate diradical character (right). (D) Structures and TPA properties of bisphenalenyl derivatives (left) and benzo-thia-fused [*n*]thienoacenequinodimethane (right).

the pseudo Jahn–Teller effect.[15,16] Molecules with intermediate diradical character, referred to as diradicaloids, serve as effective SWIR absorbers, with closed-shell and open-shell resonance structures that reflect their degree of open-shell character (Fig. 1A).[17–20] This property is quantified by the diradical character (y_0), where a value of 1 indicates a fully open-shell state, and 0 indicates a fully closed-shell state and 1–y_0 means its bond order.[21] Following the pioneering work of Chichibabin[22] and Müller,[23] researchers have developed a diverse range of diradicaloids with both Kekulé and non-Kekulé structures.[24–29] Recently, compounds such as diketopyrrolopyrroles[30,31] and certain polymers[32,33]—previously considered closed-shell—have exhibited intermediate diradical character, broadening the potential of organic materials for SWIR absorption.

In diradicaloids, the π bonds can be considered partially dissociated due to the contribution of the diradical forms, making the electron density along the π-conjugated system more susceptible to distortion under electromagnetic fields induced by high-intensity laser irradiation. As a result, they exhibit intense two-photon absorption (TPA), which is a third-order nonlinear optical (NLO) process involving the simultaneous absorption of two photons through a virtual state in response to laser irradiation (Fig. 1B).[34–36] As an illustration of the substantial influence of intermediate diradical character on TPA properties, Kamada *et al.* demonstrated that the TPA cross-section of a bis(acridine) dimer, which exhibits intermediate diradical character in its oxidized state, is over two orders of magnitude higher than that of the corresponding dimer in its lower oxidation state, which possesses a closed-shell electronic configuration (Fig. 1C).[37] Similarly, bisphenalenyl and benzo-thia-fused [*n*]thienoacenequinodimethane derivatives, which also exhibit intermediate diradical character, show large TPA cross-sections (Fig. 1D).[38,39]

For closed-shell molecules, it is well-established both extending π-conjugated systems and incorporating donor–acceptor structures can enhance the TPA cross section.[36,40] In addition to these two axes of molecular design, which form a 2D-plane containing closed-shell molecules, the diradical character can be the third axis of the degrees of freedom, which expanded the dimensionality of the molecular design (Fig. 2A). With this third axis, further enhancement of TPA can be expected. This strategy is expected to promote the development of TPA materials for applications such as three-dimensional laser microfabrication,[41–44] 3D fluorescent imaging,[44,45] and photodynamic therapy.[45–49]

We previously demonstrated that croconaine dyes, featuring a five-membered oxocarbon ring and a (thio)pyrylium skeleton (**CR1a** and **CR1b**) exhibited intermediate diradical character (y_0 = 0.63, 0.70 respectively) and showed strong TPA in the SWIR region ($\sigma^{(2)}$ = 750 GM at 1290 nm as the maximum of **CR1b**) (Fig. 2B).[50] This is the first report on the intermediate diradical character and TPA properties of croconaine dyes to our best knowledge. This report suggests that croconaine dyes have potential as excellent TPA materials, similar to polymethine dyes such as cyanine dyes, which exhibit relatively intense TPA.[51–53] In contrast to polymethine dyes, croconaine dyes exhibit an additional axis of diradical character, in addition to the extension of the π-conjugated system and the modulation of the donor and acceptor strengths in the chromophore. These properties can be fine-tuned by replacing the oxygen atom in the pyrylium skeleton with a heavier heteroatom, such as sulfur in a thiopyrylium skeleton.[50,54–56] As illustrated in Fig. 2A with blue/red arrows, tuning of the degree of intermediate diradical character by replacing heavy atom and expansion of the

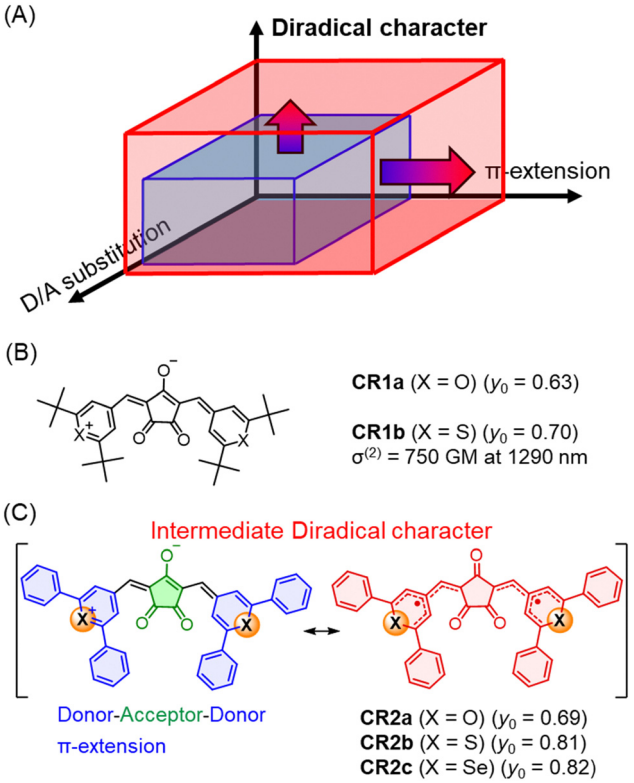

Fig. 2 (A) Design axes of molecular TPA materials: donor–acceptor substitution, π-extension, and diradical character. (B) Structures, diradical character (y_0), and TPA properties of previously reported croconaine dyes (**CR1a** and **CR1b**). (C) Structures of croconaine dyes containing phenyl-substituted chalcogenopyrylium components (**CR2a–c**).

π-conjugation have possibility of further enhancement of the TPA properties. These factors also enable the fine-tuning of the transition energy associated with TPA.

In this study, we synthesized croconaine dyes by replacing chalcogen atom in the chalcogenopyrylium ring from O to S, to Se for wider tuning diradical charter, enhancing both one-photon absorption (OPA) and TPA in the SWIR region (Fig. 2C). Additionally, we functionalized the chalcogenopyrylium core by introducing phenyl groups at the 2,5-positions to extend the π-conjugation, aiming to achieve a further red shift in both OPA and TPA. We investigated the effects of both the substitutions of chalcogen elements and phenyl groups on the intermediate diradical character, as well as the combined impact of the intermediate diradical character and the extended π-conjugated system on the OPA and TPA behaviors.

Results and discussion

Synthesis and diradical character

Croconaine dyes with oxygen (**CR2a**), sulfur (**CR2b**), and selenium (**CR2c**) as chalcogen atoms were synthesized by condensation of croconic acid with the corresponding chalcogenopyrylium perchlorates (see ESI†). In solution, these dyes exhibited no evidence of degradation under conditions of complete darkness. (Fig. S1, ESI†). Thermal gravimetric analysis of the solid-state samples revealed that the dyes possess high thermal stability (Fig. S2, ESI†). These stability data validate the reliability of the subsequent measurements. The diradical character y_0 for the optimized structures of **CR2a–c**, obtained at the CAM-UB3LYP/6-31G(d,p) level, was calculated using spin-projected unrestricted Hartree–Fock (PUHF) theory with a 6-31G(d,p) basis set.[57] The resulting values for **CR2a**, **CR2b**, and **CR2c** were y_0 = 0.69, 0.81, and 0.82, respectively.

X-Ray structures

A single crystal of **CR2c** was successfully obtained through the solvent diffusion method with a 1,1,2,2-tetrachloroethane-hexane system. The X-ray crystal structures of **CR2c** are shown Fig. 3, with detailed data provided in the ESI.† **CR2c** has a structure in which the central cyclopentenetrione and the selenopyrylium components are coplanar in a cisoid configuration. The four phenyl groups on the selenopyrylium are oriented at a dihedral angle of approximately 20° and 32° relative to the molecular plane (Fig. 3A). **CR2c** forms a dimer with a nearest-neighbor distance of 3.18 Å, and the dimers stack with a separation of 3.36 Å (Fig. 3B). Thus, the high planarity of **CR2c** promotes π–π stacking interactions in the crystal, leading to dimer formation and resulting in the dense packing of the dimers.

As mentioned earlier, molecules with intermediate diradical character exhibit both closed-shell and open-shell contributions, and the relative contribution of each resonance structure, with its distinct electron configuration, influences the bond lengths.[37] **CR2c** is expected to have multiple resonance structures due to its extended π-electron system (Fig. S4, ESI†). These structures can be classified into two zwitterionic forms, α and β, in closed-shell configurations, and two diradical forms, where unpaired electrons are delocalized over the central five-membered ring (γ) or the selenopyrylium ring (δ, Fig. 3C). Now, we focus on the outer bonds (a, d) and the inner bonds (b, c) connecting the central five-membered ring and the selenopyrylium ring, and quantify the bond length difference, ΔD = ave. (a, d) − ave. (b, c) (Fig. 3A and Table 1).

In the two closed-shell zwitterionic forms (α, β), bonds a and d (or b and c) are assigned as a pair of a double bond and a single bond, resulting in ΔD being zero. The diradical form γ, however, exhibits a negative ΔD value, as the inner bonds (b, c) are single bond and the outer bonds (a, d) are double bond. In the δ form, a positive ΔD value is observed in this bond length analysis. Actually, the X-ray structure of **CR2c** confirms a positive ΔD value, suggesting that the δ form, where the unpaired electron is delocalized on the selenopyrylium ring, has a greater contribution among the four resonance forms. Additionally, we compared the ΔD values of the DFT-optimized structures of the closed-shell singlet and open-shell triplet states with those obtained from the X-ray data. The value from the X-ray structure (+0.016) was found to lie between those of the closed-shell singlet (+0.013) and open-shell triplet states (+0.047), further supporting the intermediate diradical character of **CR2c**.

The spin density distributions of the croconaine dyes were calculated at the unrestricted CAM-B3LYP/6-31G level

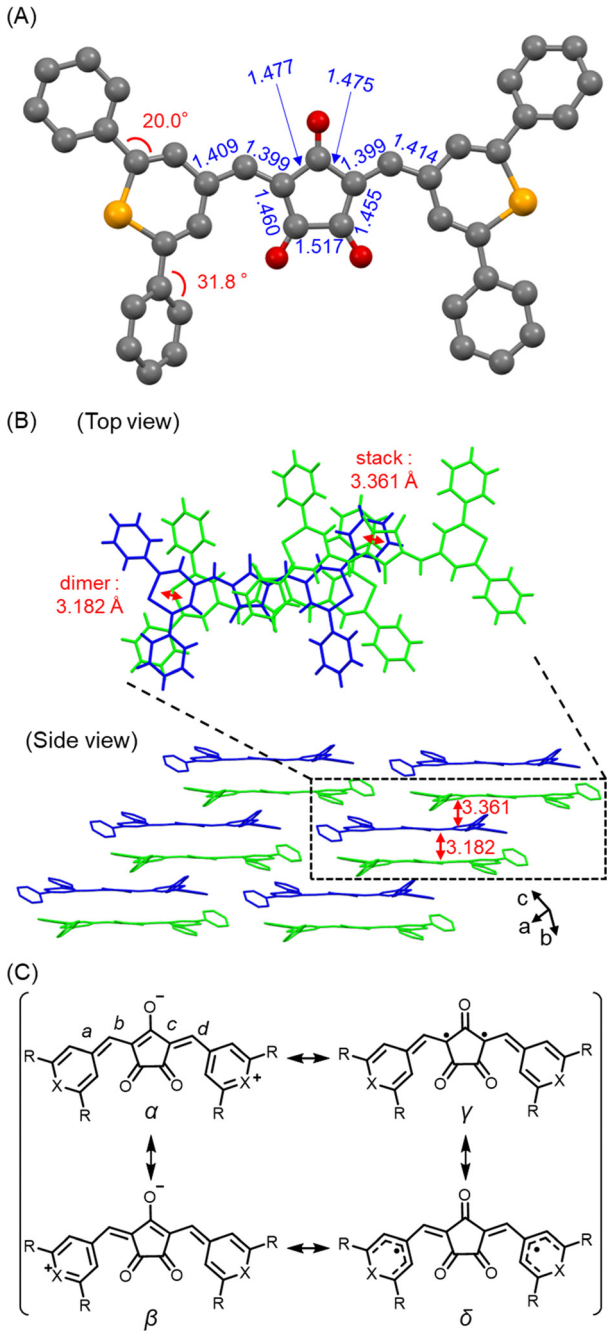

Fig. 3 (A) A single crystal X-ray structure of **CR2c** at 100 K, showing C–C bond lengths (in Å) and dihedral angles along the phenyl groups. Solvent molecules were omitted for clarity. (B) Its packing structure (top and side views) with nearest-neighbor distances highlighted in red. (C) Resonance structures of **CR2a–c**.

Table 1 Differences in average bond lengths (ΔD = ave. (a, d) − ave. (b, c)) from X-ray and optimized structures of **CR2c**[a]

	Closed-shell singlet[b]/Å	X-ray	Open-shell singlet[c]/Å	Open-shell triplet[c]/Å
ave. (a, d)	1.403	1.412	1.415	1.421
ave. (b, c)	1.390	1.396	1.380	1.374
ΔD	+0.013	+0.016	+0.035	+0.047

[a] ave. (a, b) represents the average bond length of bonds a and b. [b] Calculated at CAM-RB3LYP/6-31G(d,p) levels. [c] Calculated at CAM-UB3LYP/6-31G(d,p) levels.

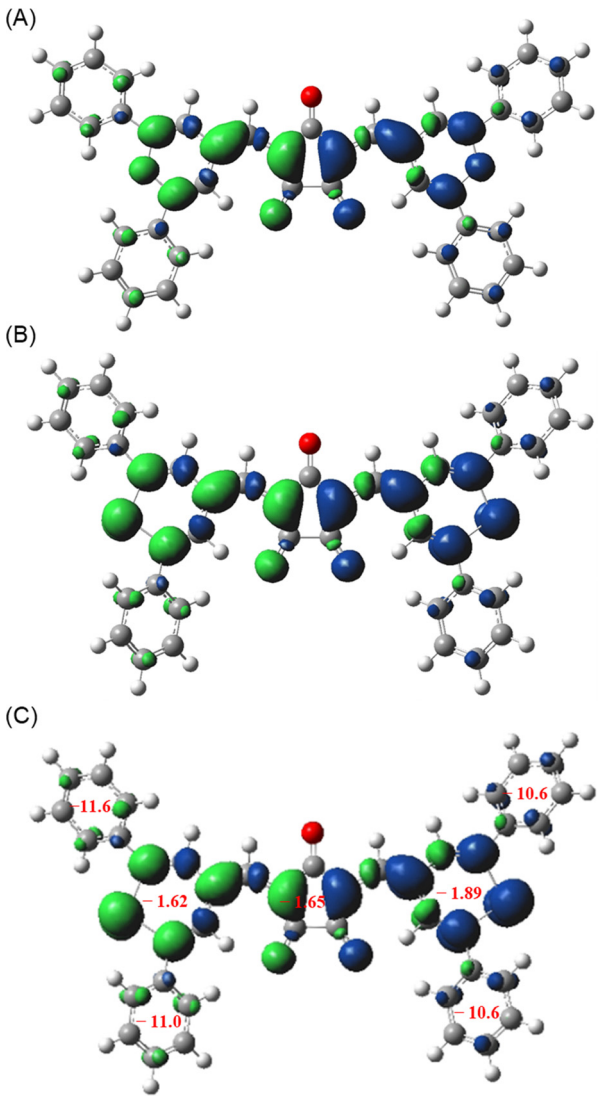

Fig. 4 Mulliken spin density maps of open-shell singlet states for **CR2a** (A), **CR2b** (B) and **CR2c** (C), calculated at the CAM-UBLYP/6-31G(d,p) level of theory with an isovalue of 0.002 (green: up spin; blue: down spin). The calculation for **CR2c** was performed using the X-ray structure, while **CR2a–b** were based on DFT-optimized structures. NICS(1)$_{zz}$ values for the selenopyrylium rings, phenyl groups, and five-membered ring, calculated at the GAIO UB3LYP/6-31G level, are shown in red.

to investigate their spin delocalization (Fig. 4). The calculations revealed that spins are delocalized over the entire molecule, including the phenyl groups attached to the pyrylium moieties. Moreover, NICS(1)$_{zz}$ values were calculated to evaluate the aromaticity of each ring.[58] The peripheral phenyl rings showed NICS(1)$_{zz}$ values below −10, confirming that they are aromatic, while the central cyclopentenetrione and chalcogenopyrylium rings exhibited values between −1.9 and −1.6, indicating reduced aromaticity (as shown in Fig. 4C).

NMR and ESR studies

The ^{1}H NMR spectra of these dyes displayed characteristics of molecules with intermediate diradical character. As a representative case, variable temperature (VT)-^{1}H NMR spectra of **CR2c** in $CDCl_3$ are shown in Fig. 5. Although sharp signals for protons at aromatic groups were observed at 213 K, they gradually broadened as the temperature increased, and completely disappeared at 313 K. The observed temperature dependence of ^{1}H NMR is typical of diradicaloids, which have a contribution of thermally populated triplet species. The similar temperature dependence of the ^{1}H NMR spectra was observed for **CR2a** and **CR2b** (Fig. S5 and S6, ESI†). However, the temperature at which the signal disappeared varied among the compounds. **CR2a** showed the signal disappearance at 333 K, whereas **CR2b** and **CR2c** exhibited it at 313 K. This difference is likely due to the varying triplet energy levels, suggesting that **CR2b** and **CR2c** are thermally excited to their triplet states at lower temperatures than **CR2a**.

Furthermore, the electron spin resonance (ESR) spectra of each dye were recorded to confirm the presence of unpaired electrons arising from thermally populated triplet states (Fig. 6A). In 1,1,2,2-tetrachloroethane at 303 K, **CR2c** displayed a broad ESR signal at g = 2.003. Unlike the behavior observed in the ^{1}H NMR spectra, the ESR signal intensified with increasing temperature, indicating the presence of unpaired electrons from a thermally populated triplet state. In the solid state, **CR2c** exhibited a more complex ESR signal than in solution (Fig. 6B). X-Ray crystal structure analysis revealed intermolecular interactions in the crystalline state for **CR2c**. These interactions are thought to influence electron spin coupling in the solid state, leading to the observed changes in the ESR signal.

A similar trend was observed for the solutions of **CR2a** and **CR2b**, which also exhibited the increase in the ESR intensities upon heating (Fig. S8, ESI†). The plots of ESR signal intensity (I_{ESR}) multiplied by temperature (T) as a function of temperature are shown in Fig. 6C. For all three dyes, $I_{ESR}T$ increased with an increase in temperature. To estimate the energy difference between the singlet and thermally accessible triplet states (ΔE_{S-T}), the data were fitted to the Bleaney–Bowers equation (see ESI†).[59] The curve-fitting analysis yielded ΔE_{S-T} values of 0.169, 0.164, and 0.148 eV for **CR2a**, **CR2b**, and **CR2c**, respectively. These results show a trend where the ΔE_{S-T} decreases as the atomic number of the chalcogens increases. The relatively small ΔE_{S-T} values suggest weak electron–electron interactions within the molecule, accompanied by a substantial contribution from the diradical form. Thus, the contribution of diradical forms increases in the order of **CR2a**, **CR2b**, and **CR2c**, which is consistent with the trend observed in the diradical character y_0 obtained from quantum chemical calculations.

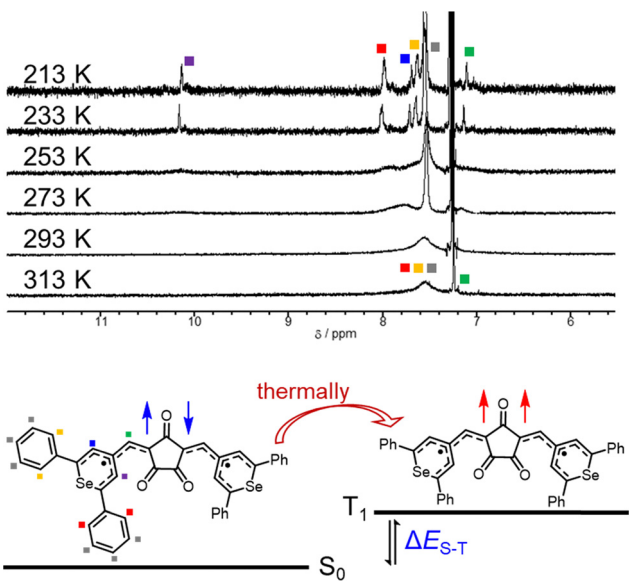

Fig. 5 Variable temperature ^{1}H-NMR spectra ($CDCl_3$, 213–313 K) of **CR2c** along with a diagram illustrating thermal excitation from singlet to triplet states.

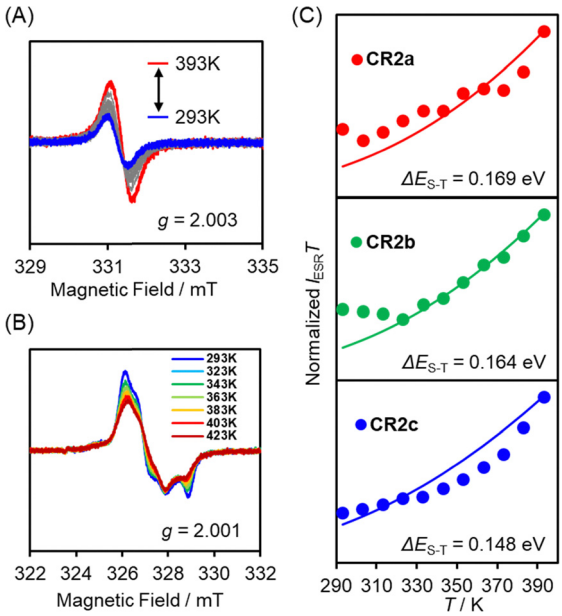

Fig. 6 ESR spectra of the solution sample in 1,1,2,2-tetrachloroethane (A, g = 2.003) and the solid sample (B, g = 2.001) of **CR2c**. Temperature–$I_{ESR}T$ plots based on ESR data of the solution samples of **CR2a** (red), **CR2b** (green), and **CR2c** (blue) (C). The lines are the fitted plots by using the Bleaney–Bowers equation.

One-photon absorption and fluorescence properties

The OPA and fluorescence emission spectra of **CR2a–c** in $CHCl_3$ are shown in Fig. 7. Detailed data, including absorption and emission maxima as well as molar extinction coefficients, are provided in Table 2. **CR2a** and **CR2b** exhibit absorption maxima at 955 nm and 1047 nm, respectively, with corresponding molar extinction coefficients of 3.3×10^5 and 1.8×10^5 M^{-1} cm^{-1}. These OPA bands are red-shifted by approximately 100 nm (360 cm^{-1} for **CR2a** and 477 cm^{-1} for **CR2b**) compared to those of the *tert*-butyl-substituted chalcogenopyrylium analogues,[49] mainly due to the π-conjugation extension by the substitution of *tert*-butyl groups with phenyl groups. The OPA maximum of **CR2c**, which contains a selenopyrylium moiety, was red-shifted

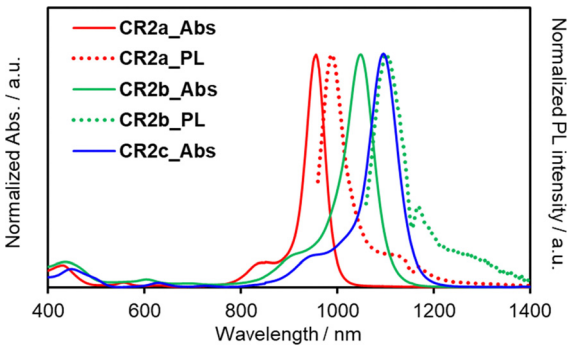

Fig. 7 Normalized electronic absorption spectra (solid line) and emission spectra (dot line) ($CHCl_3$, r.t., conc. 5×10^{-6} M) of **CR2a** (red), **CR2b** (green), and **CR2c** (blue).

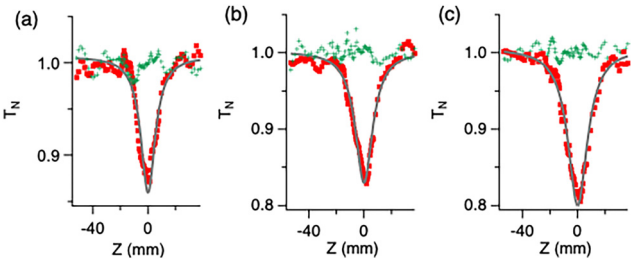

Fig. 8 Open-aperture Z-scan traces, the normalized transmittance T_N curves against the sample position z, of (a) **CR2a**, (b) **CR2b**, and (c) **CR2c** in $CHCl_3$ (0.44, 0.49, and 0.47 mM) at 1255, 1395, and 1454 nm (red square) with theoretical fits (grey curves, see ESI†) and blank solvent (green cross) at different excitation intensity I_0 of 190, 153, and 158 GW cm^{-2}, respectively.

by 49 nm (427 cm^{-1}) relative to **CR2b**, reaching 1096 nm. TD-DFT calculations for **CR2a–c** reveal that the absorption maxima of these dyes correspond to S_0–S_1 transitions, with the dominant contribution arising from the electronic transitions between the HOMOs and LUMOs (see ESI,† Table S3).

These results demonstrate that the extension of π-conjugation through the phenyl substitution, coupled with the orbital expansion by the heavy chalcogen elements, contributes to the observed red-shift and enables SWIR absorption in these dyes. Fabian *et al.* predicted a correlation between diradical character and transition energy, describing that an increase in diradical contribution leads to a decrease in transition energy. Consistent with this prediction, the diradical character increases in the order **CR2a** < **CR2b** < **CR2c**, while their transition energies decrease in the reverse order **CR2a** > **CR2b** > **CR2c**. According to the energy band gap law, organic compounds with transition energies in the SWIR region are expected to show weak fluorescence.[60] As anticipated, **CR2c**, which has the lowest transition energy, exhibited negligible fluorescence at r.t.

In contrast, **CR2a** and **CR2b** exhibited fluorescence in the SWIR region with maxima (λ_{em}) at 989 nm and 1102 nm, respectively, although their quantum yields were too low to evaluate. Thus, it remains difficult to achieve substantial SWIR emission in this class of dyes.

Two-photon absorption properties

From the above studies, it was shown that the croconaine dyes in this work exhibit intermediate diradical character, and the relative degree of their diradical contributions has been clarified. Based on this, we investigated the correlation between diradical character and TPA properties. The TPA properties of **CR2a–c** were examined using the femtosecond Z-scan technique (see ESI†). Representative Z-scan traces are presented in Fig. 8. The excitation intensity dependence proved the nonlinear absorption signal (dip in the trace) originated from TPA process (Fig. S9–S11, ESI†). By scanning the wavelength, their TPA spectra were obtained. All dyes exhibited a distinct, intense TPA band in the SWIR region (Fig. 9, Table 2), with TPA maxima observed at 1255, 1395, and 1445 nm for **CR2a**, **CR2b**, and **CR2c**, respectively. This trend in TPA transition energies aligns with the order observed for OPA transitions, showing an inverse correlation with diradical character. It is also noted here that the TPA transition energies differ from those of the OPA maxima, which shows Laporte's symmetry selection rule holds.[36] In other words, these dyes are virtually centrosymmetric on the π-conjugation backbone.

The OPA and TPA spectra of **CR2a–c** were simulated by DFT calculations at the CAM-B3LYP/6-31G(d,p) level (see ESI†). Although the transition energies were slightly overestimated for OPA and significantly overestimated for TPA, the relative spectral positions of OPA and TPA bands matched well with experimental values (Fig. S12, ESI†). The simulations suggest that the OPA and TPA transitions correspond to the $S_1 \leftarrow S_0$ and $S_4 \leftarrow S_0$ states, respectively, which supports observed fact that the transition energies of the TPA maxima differed from those of the OPA maxima. In the simulation, the relatively weak second OPA band appears on the shorter wavelength side of the TPA band assigned to the $S_4 \leftarrow S_0$ transition. In the experimental spectrum of each dye, the substantial TPA is also

Table 2 Differences in average bond lengths (ΔD = ave. (*a*, *d*) − ave. (*b*, *c*)) from X-ray and optimized structures of **CR2c**[a]

Dye	λ_{OPA}[a]/nm	ε[b]/10^5 M^{-1} cm^{-1}	λ_{PL}[c]/nm	Stokes shift/cm^{-1}	λ_{TPA}[d]/nm	$\sigma^{(2)}$[e]/GM
CR2a	955	3.30	989	360	1255	1008 ± 136
CR2b	1047	1.83	1102	477	1395	1011 ± 202
CR2c	1096	1.64	N.D.	N.D.	1445	1177 ± 193

[a] OPA maxima in $CHCl_3$ (conc. 5×10^{-6} M). [b] Molar absorption coefficient. [c] Emission maxima in $CHCl_3$ (conc. 5×10^{-6} M, excitation at 430 nm). [d] TPA maxima in $CHCl_3$ (conc. 0.44 mM for **CR2a**, 0.49 mM for **CR2b**, and 0.47 mM for **CR2c**) obtained by Z-scan technique. [e] TPA cross section ($\sigma^{(2)}$) was expressed in the Göppert-Mayer (GM) unit defined as 1 GM = 10^{-50} cm^4 s $molecule^{-1}$ $photon^{-1}$.

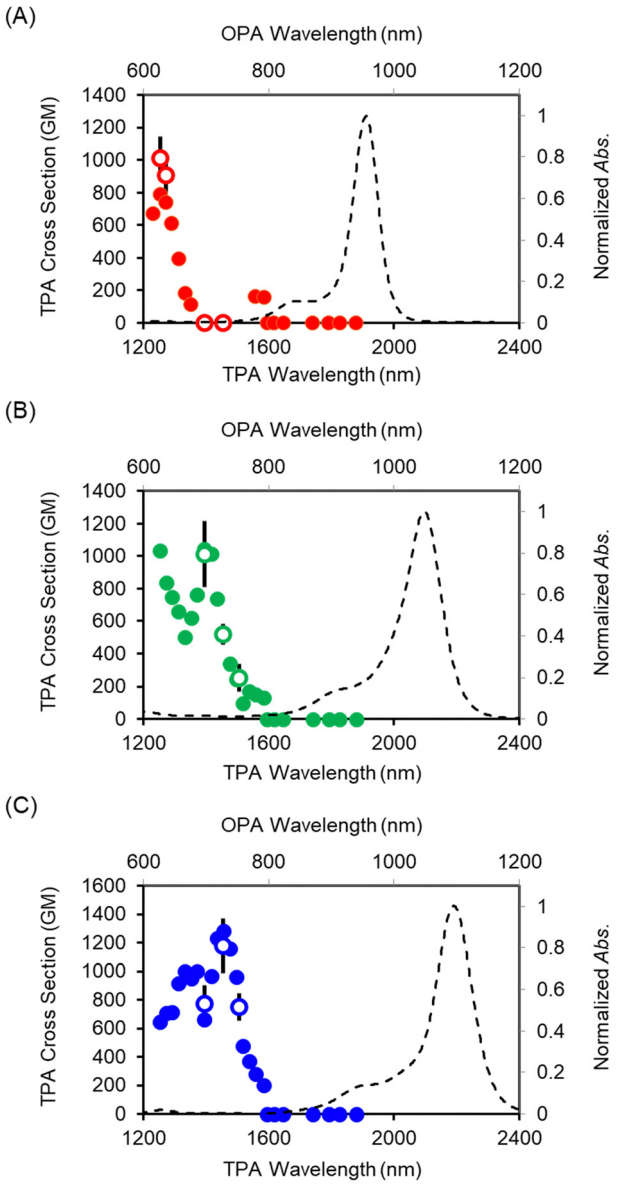

Fig. 9 TPA spectra in the cross section $\sigma^{(2)}$ (symbols, left and bottom axes) of **CR2a** (A), **CR2b** (B) and **CR2c** (C) in $CHCl_3$ together with the corresponding OPA spectra (black dashed line, right and top axes). λ_{TPA} comes at the same horizontal position of $2 \times \lambda_{OPA}$, resulting in the same transition energies for TPA and OPA comes at the same horizontal position. Open symbols and the filled symbols with error bars mean that the $\sigma^{(2)}$ data were obtained by the different measurement procedures (wavelength scan and power scan, respectively; see the ESI† for details.).

observed on the shorter wavelength side of the strong $S_4 \leftarrow S_0$ TPA band, likely due to resonant enhancement by the OPA.[61,62]

The peak $\sigma^{(2)}$ of **CR2a**, **CR2b**, and **CR2c** of the band were determined to be 1008 ± 136, 1011 ± 202, and 1177 ± 193 GM, respectively (where 1 GM = 10^{-50} cm^4 s $molecule^{-1}$ $photon^{-1}$). These are significant values in the SWIR region as this size of molecule. To compare with the benchmarks, Fig. 10 shows the reported $\sigma^{(2)}$ scaled by molecular weight (M.w.) for structurally similar oxocarbon analogues (squaraine dyes **SQ1b** and a previously repored croconaine dye with shorter conjugation **CR1b**,

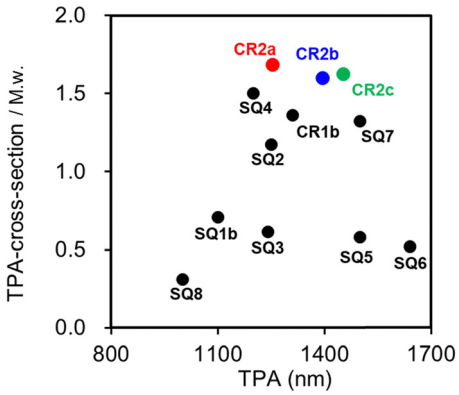

Fig. 10 Plot of the maximum TPA wavelength *versus* TPA cross section for each dye divided by molecular weight for squaraine and croconaine dyes (detail showed in Fig. S14 and Table S5, ESI†).

see Fig. S14 for their structures, ESI†) is plotted against the TPA peak wavelength. Clearly, it is shown that **CR2a–c** have the highest class values of $\sigma^{(2)}$/M.w. in the SWIR region, compared to the closed-shell squaraine dye. This finding suggests that these croconaine dyes possess unusually large $\sigma^{(2)}$, likely due to their extended conjugation and strong donor–acceptor interactions. Furthermore, the intermediate diradical character of these dyes contribute to the observed enhancement of $\sigma^{(2)}$.

Conclusions

This study highlights the relationships between intermediate diradical characters and the OPA and TPA properties of croconaine dyes with phenyl-substituted chalcogenopyrylium components (O, S, and Se) in the short-wavelength infrared (SWIR) region. X-Ray crystallography revealed that the phenyl groups are not completely orthogonal to the chalcogenopyrylium ring, which likely contributes to the expansion of the π-conjugated system. Bond length analysis based on X-ray data, along with VT ESR and NMR measurements, indicated that these croconaine dyes exhibit intermediate diradical character. The contribution of the diradical forms increased as the chalcogen atoms became heavier (O < S < Se). Due to the extended π-conjugation and intermediate diradical character, these dyes exhibit strong OPA in the SWIR region The enhanced diradical character, driven by heavier chalcogen atoms, lowers the transition energy for both OPA and TPA, while also increasing the TPA cross section. These findings suggest that, besides adjusting the extent of π-conjugation, the third axis of diradical character can be fine-tuned to optimize the OPA and TPA properties of croconaine dyes, making these dyes more effective for SWIR-based applications.

Author contributions

T. O. and T. M. designed experiments, conducted synthesis of compounds, analysed data, and wrote the manuscript. D. S. and H. F. conducted X-ray crystallographic analysis, collected

ESR spectra, and analysed data of ESR. N. S., S. K. and S. Y. conducted characterization of compounds. L. M. and K. K. collected and analysed OPA/TPA spectra. All authors reviewed the manuscript and agreed to its publication.

Data availability

All data associated with this article are available in the main text and ESI.†

Conflicts of interest

There are no conflicts to declare.

Acknowledgements

This work was supported by JSPS KAKENHI Grant Numbers 24K01573, ENEOS Tonengeneral Research/Development Encouragement & Scholarship Foundation, Iketani Science and Technology Foundation, and JST, the establishment of university fellowships towards the creation of science technology innovation, Grant Number JPMJFS2138.

Notes and references

1 Z.-Y. Yang, Y.-F. Zhao, Y.-Y. Zhou, J.-W. Qiao, Y.-C. Chuang, M. S. Molokeev and Z.-G. Xia, *Adv. Funct. Mater.*, 2022, **32**, 12.
2 J. Qiao, G. Zhou, Y. Zhou, Q. Zhang and Z. Xia, *Nat. Commun.*, 2019, **10**, 5267.
3 R. X. Wang, Y. Ou, Y. Chen, T.-B. Ren, L. Yuan and X. B. Zhang, *J. Am. Chem. Soc.*, 2024, **146**, 11669–11678.
4 C. Y. Li, G. C. Chen, Y. J. Zhang, F. Wu and Q. B. Wang, *J. Am. Chem. Soc.*, 2020, **142**, 14789.
5 J. Huang and K. Pu, *Angew. Chem., Int. Ed.*, 2020, **59**, 11717.
6 T. Sheikh, W. J. Mir, A. Alofi, M. Skoroterski, R. Zhou, S. Nematulloev, M. N. Hedhili, M. B. Hassine, M. S. Khan, K. E. Yorov, B. E. Hasanov, H. Liao, Y. Yang, A. Shamim, M. Abulikemu, O. F. Mohammed and O. M. Bakr, *J. Am. Chem. Soc.*, 2024, **146**, 29094–29103.
7 H. Jalali, L. De Trizio, L. Manna and F. Di Stasio, *Chem. Soc. Rev.*, 2022, **51**, 9861–9881.
8 X. Guan, X. Yu, D. Periyanagounder, M. R. Benzigar, J. K. Huang, C. H. Lin, J. Kim, S. Singh, L. Hu, G. Liu, D. Li, J. H. He, F. Yan, Q. J. Wang and T. Wu, *Adv. Opt. Mater.*, 2021, **9**, 2001708.
9 L. M. Obloy, S. Jockusch and A. N. Tarnovsky, *Phys. Chem. Chem. Phys.*, 2024, **26**, 24261–24278.
10 A. L. Antaris, H. Chen, K. Cheng, Y. Sun, G. Hong, C. Qu, S. Diao, Z. Deng, X. Hu, B. Zhang, X. Zhang, O. K. Yaghi, Z. R. Alamparambil, X. Hong, Z. Cheng and H. Dai, *Nat. Mater.*, 2016, **15**, 235–242.
11 Q. Yang, Z. Ma, H. Wang, B. Zhou, S. Zhu, Y. Zhong, J. Wang, H. Wan, A. Antaris, R. Ma, X. Zhang, J. Yang, X. Zhang, H. Sun, W. Liu, Y. Liang and H. Dai, *Adv. Mater.*, 2017, **29**, 1605497.
12 A. Ji, H. Lou, C. Qu, W. Lu, Y. Hao, J. Li, Y. Wu, T. Chang, H. Chen and Z. Cheng, *Nat. Commun.*, 2022, **13**, 3815.
13 Q. Wu, Z. Kang, Q. Gong, X. Guo, H. Wang, D. Wang, L. Jiao and E. Hao, *Org. Lett.*, 2020, **22**, 7513.
14 S. Zhu, R. Tian, A. L. Antaris, X. Chen and H. Dai, *Adv. Mater.*, 2019, **31**, 1900321.
15 D.-H. Li and B. D. Smith, *J. Org. Chem.*, 2022, **87**, 5893–5903.
16 Y. Ni and J. Wu, *Tetrahedron Lett.*, 2016, **57**, 5426–5434.
17 M. Abe, *Chem. Rev.*, 2013, **113**, 7011–7088.
18 T. Kubo, *Chem. Lett.*, 2015, **44**, 111–122.
19 N. Nakano, *Chem. Rec.*, 2017, **17**, 27–62.
20 T. Y. Gopalakrishna, W. Zeng, X. Lu and J. Wu, *Chem. Commun.*, 2018, **54**, 2186–2199.
21 K. Yamaguchi, *Chem. Phys. Lett.*, 1975, **33**, 330–335.
22 A. E. Tschitschibabin, *Chem. Ber.*, 1907, **40**, 1810–1819.
23 E. Müller and H. Pfanz, *Ber. Dtsch. Chem. Ges. B*, 1941, **74**, 1051–1074.
24 T. Kubo, A. Shimizu, M. Sakamoto, M. Uruichi, K. Yakushi, M. Nakano, D. Shiomi, K. Sato, T. Takui, Y. Morita and K. Nakasuji, *Angew. Chem., Int. Ed.*, 2005, **44**, 6564–6568.
25 A. Shimizu, R. Kishi, M. Nakano, D. Shiomi, K. Sato, T. Takui, I. Hisaki, M. Miyata and Y. Tobe, *Angew. Chem., Int. Ed.*, 2013, **52**, 6076–6079.
26 A. Arikawa, A. Shimizu, D. Shiomi, K. Sato and R. Shintani, *J. Am. Chem. Soc.*, 2021, **143**, 19599–19605.
27 A. Konishi and M. Yasuda, *Chem. Lett.*, 2021, **50**, 195–212.
28 H. Hayashi, J. E. Barker, A. Cárdenas Valdivia, R. Kishi, S. N. MacMillan, C. J. Gómez-García, H. Miyauchi, Y. Nakamura, M. Nakano, S.-I. Kato, M. M. Haley and J. Casado, *J. Am. Chem. Soc.*, 2020, **142**, 20444–20455.
29 Q. Wang, P. Hu, T. Tanaka, T. Y. Gopalakrishna, T. S. Herng, H. Phan, W. Zeng, J. Ding, A. Osuka, C. Chi, J. Siegel and J. Wu, *Chem. Sci.*, 2018, **9**, 5100–5105.
30 Z. Chen, W. Li, M. A. Sabuj, Y. Li, W. Zhu, M. Zeng, C. S. Sarap, M. M. Huda, X. Qiao, X. Peng, D. Ma, Y. Ma, N. Rai and F. Huang, *Nat. Commun.*, 2021, **12**, 5889.
31 W. Wang, L. Ge, G. Xue, F. Miao, P. Chen, H. Chen, Y. Lin, Y. Ni, J. Xiong, Y. Hu, J. Wu and Y. Zheng, *Chem. Commun.*, 2020, **56**, 1405–1408.
32 H. Cai, H. Tang, T. Wang, C. Xu, J. Xie, M. Fu, X. Luo, Z. Hu, Y. Zhang, Y. Deng, G. Li, C. Liu, F. Huang and Y. Cao, *Angew. Chem., Int. Ed.*, 2024, **63**, e202402375.
33 L. Huang, N. Eedugurala, A. Benasco, S. Zhang, K. S. Mayer, D. J. Adams, B. Fowler, M. M. Lockart, M. Saghayezhian, H. Tahir, E. R. King, S. Morgan, M. K. Bowman, X. Gu and J. D. Azoulay, *Adv. Funct. Mater.*, 2020, **30**, 1909805.
34 X. Shi, P. M. Burrezo, S. Lee, W. Zhang, B. Zheng, G. Dai, J. Chang, J. T. López Navarrete, K.-W. Huang, D. Kim, J. Casado and C. Chi, *Chem. Sci.*, 2014, **5**, 4490.
35 S. Pascal, S. David, C. Andraud and O. Maury, *Chem. Soc. Rev.*, 2021, **50**, 6613–6658.
36 M. Pawlicki, H. A. Collins, R. G. Denning and H. L. Anderson, *Angew. Chem., Int. Ed.*, 2009, **48**, 3244–3266.

37 K. Kamada, S. Fuku-en, S. Minamide, K. Ohta, R. Kishi, M. Nakano, H. Matsuzaki, H. Okamoto, H. Higashikawa, K. Inoue, S. Kojima and Y. Yamamoto, *J. Am. Chem. Soc.*, 2013, **135**, 232–241.
38 K. Kamada, K. Ohta, T. Kubo, A. Shimizu, Y. Morita, K. Nakasuji, R. Kishi, S. Ohta, S. Furukawa, H. Takahashi and M. Nakano, *Angew. Chem., Int. Ed.*, 2007, **46**, 3544–3546.
39 X. Shi, E. Quintero, S. Lee, L. Jing, T. S. Herng, B. Zheng, K.-W. Huang, J. T. López Navarrete, J. Ding, D. Kim, J. Casado and C. Chi, *Chem. Sci.*, 2016, **7**, 3036–3046.
40 E. A. Yildiz, G. Sevinç, S. Tekin, A. Karatay, M. Hayvalı and A. Elmali, *Dyes Pigm.*, 2021, **193**, 109522.
41 S. Maruo, O. Nakamura and S. Kawata, *Opt. Lett.*, 1997, **22**, 132.
42 B. H. Cumpston, S. P. Ananthavel, S. Barlow, D. L. Dyer, J. E. Ehrlich, L. L. Erskine, A. A. Heikal, S. M. Kuebler, I. Y. S. Lee, D. McCord-Maughon, J. Qin, H. Rockel, M. Rumi, X.-L. Wu, S. R. Marder and J. W. Perry, *Nature*, 1999, **398**, 51.
43 K. D. Belfield, K. J. Schafer, Y. Liu, J. Liu, X. Ren and E. W. V. Stryland, *J. Phys. Org. Chem.*, 2000, **13**, 837.
44 S. Kawata, H.-B. Sun, T. Tanaka and K. Takada, *Nature*, 2001, **412**, 697.
45 O. Varnavski and T. Goodson III, *J. Am. Chem. Soc.*, 2020, **142**, 12966–12975.
46 A. Diaspro and M. Robello, *J. Photochem. Photobiol., B*, 2000, **55**, 1–8.
47 K. Ogawa and Y. Kobuke, *Org. Biomol. Chem.*, 2009, **7**, 2241.
48 J. P. Celli, B. Q. Spring, I. Rizvi, C. L. Evans, K. S. Samkoe, S. Verma, B. W. Pogue and T. Hasan, *Chem. Rev.*, 2010, **110**, 2795.
49 Y. Shen, A. J. Shuhendler, D. Ye, J.-J. Xu and H.-Y. Chen, *Chem. Soc. Rev.*, 2016, **45**, 6725.
50 T. Maeda, T. Oka, D. Sakamaki, H. Fujiwara, N. Suzuki, S. Yagi, T. Konishi and K. Kamada, *Chem. Sci.*, 2023, **14**, 1978.
51 S. Webster, J. Fu, L. A. Padilha, O. V. Przhonska, D. J. Hagan, E. W. Van Stryland, M. V. Bondar, Y. L. Slominsky and A. D. Kachkovski, *Chem. Phys.*, 2008, **348**, 143–151.
52 Q. Bellier, N. S. Makarov, P.-A. Bouit, S. Rigaut, K. Kamada, P. Feneyrou, G. Berginc, O. Maury, J. W. Perry and C. Andraud, *Phys. Chem. Chem. Phys.*, 2012, **14**, 15299.
53 L. A. Padilha, S. Webster, O. V. Przhonska, H. Hu, D. Peceli, T. R. Ensley, M. V. Bondar, A. O. Gerasov, Y. P. Kovtun, M. P. Shandura, A. D. Kachkovski, D. J. Hagan and E. W. V. Stryland, *J. Phys. Chem. A*, 2010, **114**, 6493–6501.
54 T. Oka, T. Maeda, D. Sakamaki, N. Suzuki, S. Yagi, S. Kodama and H. Fujiwara, *Org. Chem. Front.*, 2025, **12**, 42–47.
55 W. Wang, L. Ge, G. Xue, F. Miao, P. Chen, H. Chen, Y. Lin, Y. Ni, J. Xiong, Y. Hu, J. Wu and Y. Zheng, *Chem. Commun.*, 2020, **56**, 1405–1408.
56 L. Shen, Q. Wu, J. Lu, H. Zhao, H. Liu, Q. Meng and X. Li, *J. Mater. Chem. C*, 2022, **10**, 10404–10411.
57 D. López-Carballeira, D. Casanova and F. Ruipérez, *ChemPhysChem*, 2018, **19**, 2224–2233.
58 H. Fallah-Bagher-Shaidaei, C. S. Wannere, C. Corminboeuf, R. Puchta and P. V. R. Schleyer, *Org. Lett.*, 2006, (8), 863–866.
59 B. Bleaney and K. D. Bowers, Anomalous paramagnetism of copper acetate, *Proc. R. Soc. London, Ser. A*, 1952, **214**, 451–465.
60 C. Erker and T. Basché, *J. Am. Chem. Soc.*, 2022, **144**, 14053–14056.
61 K. Kamada, K. Ohta, Y. Iwase and K. Kondo, *Chem. Phys. Lett.*, 2003, **372**, 386–393.
62 J. M. Hales, D. J. Hagan, E. W. Van Stryland, K. J. Schafer, A. R. Morales, K. D. Belfield, P. Pacher, O. Kwon, E. Zojer and J. L. Bredas, *J. Chem. Phys.*, 2004, **121**, 3152–3160.

